

06,13

Crystal structure, nanostructure, and dielectric characteristics of 0.91NaNbO₃–0.09SrZrO₃ films grown on a (001)SrTiO₃(0.5% Nb) substrate

© Ya.Yu. Matyash¹, D.V. Stryukov¹, A.V. Pavlenko^{1,2}, N.V. Ter-Oganessian²

¹ Southern Scientific Center, Russian Academy of Sciences, Rostov-on-Don, Russia

² Southern Federal University, Research Institute of Physics, Rostov-on-Don, Russia

E-mail: matyash.ya.yu@gmail.com

Received June 14, 2023

Revised August 23, 2023

Accepted August 25, 2023

The structure, nanostructure, and properties of a 0.91NaNbO₃–0.09SrZrO₃ thin film with a thickness of ~ 30 nm, grown by RF cathode sputtering in an oxygen atmosphere on a (001)SrTiO₃(0.5%Nb) substrate, have been studied. According to X-ray diffraction data, a significant tensile strain of the unit cell, which reaches 4.8%, occurs in the film in the direction perpendicular to the substrate. It is shown, that the likely film growth mechanism is the Frank–van der Merwe mechanism. The results of studying the dielectric hysteresis loops of the film in fields up to 833 kV/cm and its piezoactivity using atomic force microscopy indicated the presence of a ferroelectric response in it. Possible reasons for the identified features are discussed.

Keywords: antiferroelectric, NaNbO₃, SrZrO₃, atomic force microscopy, X-ray diffraction, dielectric spectroscopy.

DOI: 10.61011/PSS.2023.10.57223.111

1. Introduction

Antiferroelectric (AFE) materials attracted the attention of researchers for many years in practical terms and from the point of fundamental studies view [1]. In the form of thin films, AFEs have great potential for use in microelectronics. For example, under the influence of an electric field, during the phase transition between the initial AFE state and the induced ferroelectric (FE) phase, large energy is accumulated or released, which can be used in capacitors with a high density of stored energy [1]. Despite intensive studies of AFE materials and the results achieved in this area [2], questions regarding the determination of the phase transitions mechanism(s) remain unresolved. The functional materials of solid solutions (SS) based on lead zirconate titanate PbZrO₃–PbTiO₃ (PZT) for long time were the most studied and in many cases applicable materials [3]. However, due to the need to create and use environmentally friendly, Pb-free materials [4], the interest in study of lead-free AFEs increased significantly over the past 20 years. As our analysis of the publications shown, one of the most promising lead-free AFEs are SSs based on sodium niobate NaNbO₃ (NNO). This material is also interesting because it contains a record number of phase transitions for materials with a perovskite-type structure [5]. In the case of NNO single-crystals, at the points of phase transitions, noticeable changes occur in the dielectric permittivity dependence [6], and in a certain temperature range, depending on the direction and value of the field, both ordinary ferroelectric hysteresis loops and double loops characteristic of AFE

can be observed. At room temperature, NNO can be in two phases: in the AFE P-phase (sp.gr. P₆mm) or in the ferroelectric (FE) Q-phase (sp.gr. P₂1ma [7]). The Q-phase in sodium niobate can be obtained, for example, by applying an electric field or by doping [8], however, after the field removal the reverse transition to the AFE P-phase usually does not occur, since the free energy of these phases is close.

A stable AFE phase in ceramics is obtained, for example, in SS (1–x)NaNbO₃–xSrZrO₃ [9] and (1–x)NaNbO₃–xCaZrO₃ [10] at 0 < x < 0.10, and just in these materials that promising energy efficiency parameters are fixed. Currently, most of the papers relate to the study of these materials in the bulk ceramics form, and only over the last decade they were obtained and studied in the film form [11]. The influence of strains, implemented in thin films, on the structure and properties of SS based on NaNbO₃ was poorly studied, and the results are ambiguous. In this case, as it is known, the method of obtaining objects plays an important role [12].

In paper [13] we for the first time obtained heteroepitaxial thin films of SS 0.91NaNbO₃–0.09SrZrO₃ (NNSZO) on MgO(001) substrates with an intermediate electrode SrRuO₃ (SRO) by RF cathode sputtering. For the NNSZO layer, the calculated value of microstrains is low and amounts to $\varepsilon = 0.001$. The phase transition from the AFE phase to the paraelectric phase in a thin film is diffuse and arises below ~ 410 K. It was found that NNSZO films are in the AFE phase at room temperature, and with an

increase in the electric field strength, when analyzing the dielectric hysteresis loops, a phase transition from AFE to FE occurs. However, currently we are not able to study the properties of NNSZO/SRO/MgO(001) heterostructure with NNSZO film thickness of less than 100 nm due to breakdown that occurs when high voltages are applied to the sample. Preliminary studies of NNSZO/SrTiO₃(001) showed that at thickness of more than 1000 nm NNSZO films, as in [13], are in the AFE phase. This paper presents the study results of the structure, surface morphology and properties of the NNSZO thin film ~ 30 nm thick grown on a strontium titanate substrate under similar conditions. It is shown how such a small film thickness affects the formation of the surface relief and ferroelectric properties.

2. Methods of obtaining and studying objects

Gas-discharge RF deposition of 0.91NNO–0.09SZO heteroepitaxial films carried out on „Plasma 50 SE“ system. A ceramic target with a diameter of 50 mm and 3 mm thick was manufactured using traditional ceramic technology (two-stage synthesis and subsequent sintering of ceramics in air atmosphere). As substrate we used the prepared for heteroepitaxial deposition alloyed with 0.5% Nb SrTiO₃ plates (cut (001), 0.5 mm thick). Initial temperature of the substrate — 400°C, pure oxygen pressure — 0.55 Torr, RF power — 150 W, distance target-substrate — 12 mm. The ceramic target with the stoichiometric composition 0.91NaNbO₃–0.09SrZrO₃ was manufactured at the Research Institute of Physics of Southern Federal University (Russia).

X-ray diffraction studies were carried out on a multifunctional X-ray complex „RIKOR“ [goniometer with step up to 0.001° (Crystal Logic Inc.); X-ray tube BSV21-Cu (JSC „Svetlana-Roentgen“), scintillation detector (LLC ITC „Radikon“)].

The surface morphology of the thin film was studied in semi-contact and contact modes on an atomic-force microscope (AFM) „Ntegra Academia“ (NT-MDT, Russia) using a silicon cantilever NS15/50 (NT-MDT, Russia, hardness — 40 N/m, probe rounding radius — 8 nm). Scanning of the surface relief fragment of size 10 × 10 μm² with a resolution of 300 points per line was carried out at a rate of 1 Hz in semi-contact mode. For the fragment 2 × 2 μm² with a resolution of 300 points per line in contact mode the rate was 0.8 Hz. Using a silicon cantilever NSG01 with Pt coating (NT-MDT, Russia) in the Kelvin probe force microscopy (KPFM) the surface potential of the film from pre-polarized areas was recorded. Processing and analysis of the received scans were carried out in the Image Analysis program.

For dielectric measurements the out-of-plane capacitor structures were formed: the upper electrode was Ag/Pd

layer deposited by magnetron sputtering in argon atmosphere on Emitech SC7620 setup through a mask with a hole diameter of 60 μm. Relative dielectric permittivity ϵ was determined from the ratio $C = \epsilon\epsilon_0 S/h$, where C — structure capacitance, h — ferroelectric layer thickness, S — electrode area, $\epsilon_0 = 8.854 \cdot 10^{-12}$ F/m — electric constant. The electrode area was measured using a KeyenceVK-9700 3D microscope (Joint Center for Scientific and Technological Equipment of Southern Scientific Center of the Russian Academy of Sciences). The $P(E)$ dependencies at frequency of 1 kHz were measured using a measuring setup, which included „TFAnalyzer2000“ and temperature chamber „Linkam THMS600 stage“.

3. Experimental results and discussion

The crystal structure of NNSZO film was studied by X-ray diffraction. θ – 2θ X-ray diffraction pattern of the heterostructures (Figure 1) contains only reflections from NNSZO film and STO substrate, which indicates the crystalline impurities absence in the film.

The presence of the (00L) family reflections of the film proves that the [001] crystallographic axes of the film and the substrate are co-directional. The full width at half maximum of (001) reflection is 0.29°, which, according to Scherrer's formula, corresponds to film thickness of 30 nm. The out-of-plane lattice constant is $c = 4.11$ Å. The low intensity of reflections associated with the small thickness of NNSZO film and the small size of the coherent scattering regions did not allow us to determine the in-plane lattice constants, and the epitaxial relationships between the film and the substrate.

The magnitude and sign of internal stresses (arising directly during the heterostructure formation) in thin films depend on a number of factors such as mismatch between the lattice constants of the film and substrate, the occurrence of point defects, the introduction of impurities [14,15], most of which relate to application conditions and methods. The tensile strain of the unit cell of the NNSZO film along (001) direction relative to the ceramic unit cell was significant and

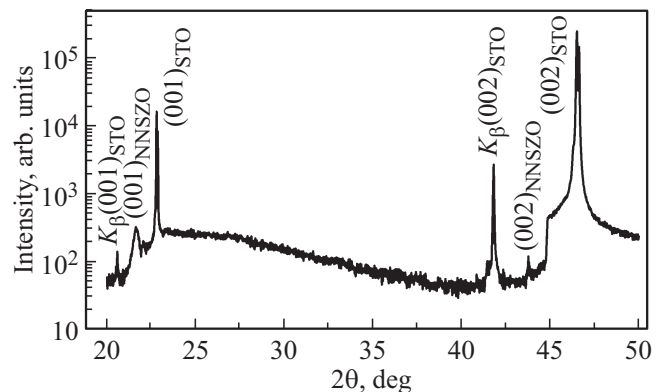


Figure 1. θ – 2θ -X-ray pattern of NNSZO/STO heterostructure.

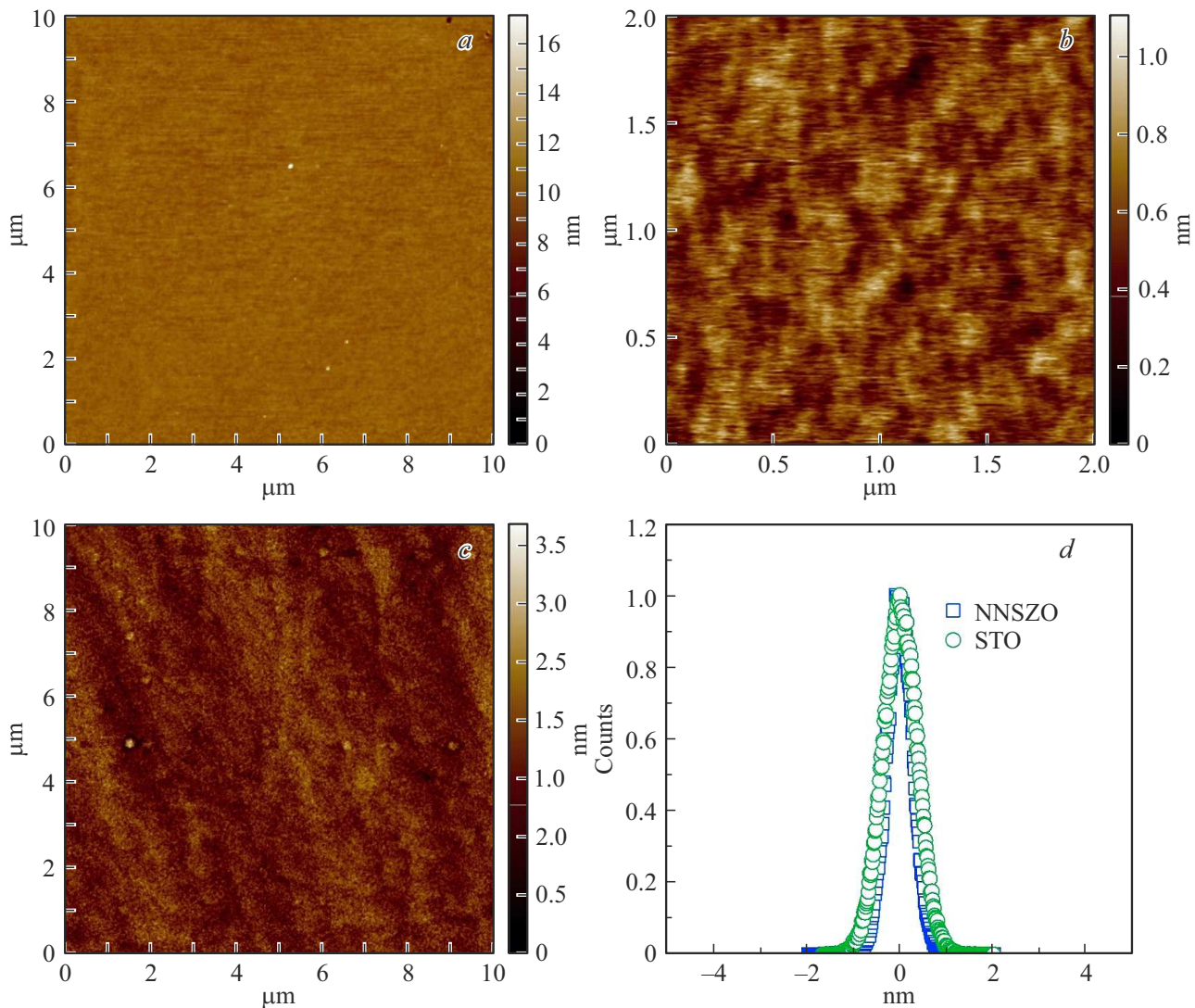


Figure 2. NNSZO film topography in semi-contact (*a*) and contact (*b*) modes, STO substrate in semi-contact mode (*c*) and histogram of height distribution over the surface of the film and substrate (*d*).

amounted to $\sim 4.8\%$ (for a bulk sample $c_{\text{bulk}} = 3.921 \text{ \AA}$), which allows us to expect a significant change in properties of material.

AFM images of NNSZO film surface are shown in Figure 2. It can be seen that the surface of NNSZO film is homogeneous and does not contain cracks, pores, voids, traces of impurity phases and other growth defects. For the surface fragment of size $10 \times 10 \mu\text{m}^2$ the root-mean-square roughness value for the film $\sim 30 \text{ nm}$ thick was 0.3 nm only.

Additionally, a more detailed scanning of the region $2 \times 2 \mu\text{m}^2$ was carried out in contact mode (Figure 2, *b*), which confirmed that the surface of NNSZO film is smooth, and the height difference is less than 1.2 nm . When comparing the relief degree of STO substrate and NNSZO/STO(001) heterostructure it is clear (Figure 2, *d*), that they are comparable — the histograms of height distribution over the surface for them practically coincide, and the root-mean-square roughness of the substrate surface

was 0.37 nm , which is close to the roughness value for the film. Taking into account the X-ray diffraction data, the results indicate that the studied NNSZO films on STO(001) substrate were most likely grown according to the Frank-van der Merwe growth mechanism (layer-by-layer growth) [14]. This growth mechanism occurs when the sum of the film surface energy and the film/substrate interface energy is less than the surface energy of the substrate. Exactly with this growth mechanism the significant strains of the unit cell are realized in films [14], which was mentioned above.

To study the ferroelectric properties of the grown films, we studied their local piezoactivity using an AFM „Ntegra Academia“ in the KPFM. To perform this, first, in contact mode, on the fragment $5 \times 5 \mu\text{m}^2$ the rectangular regions of size $1.5 \times 2 \mu\text{m}^2$ were polarized along the contour with a constant voltage $+6 \text{ V}$ and -6 V (Figure 3).

Then, using a two-pass technique (in the second pass the probe was moved away from the surface by 10 nm , the

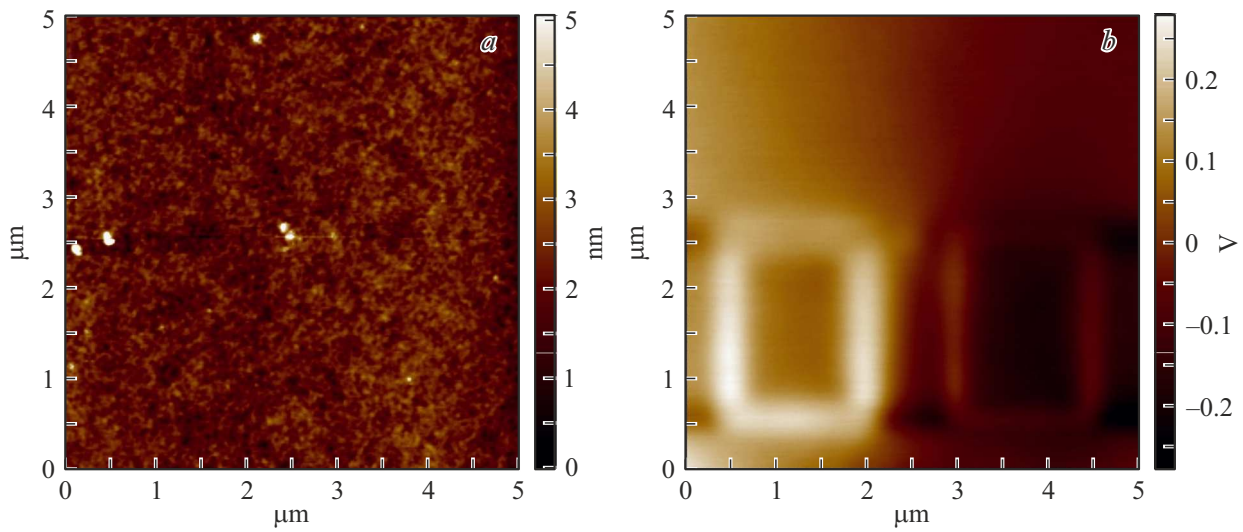


Figure 3. Topography (*a*) and surface potential signal obtained in the KPFM (*b*) of the NNSZO film.

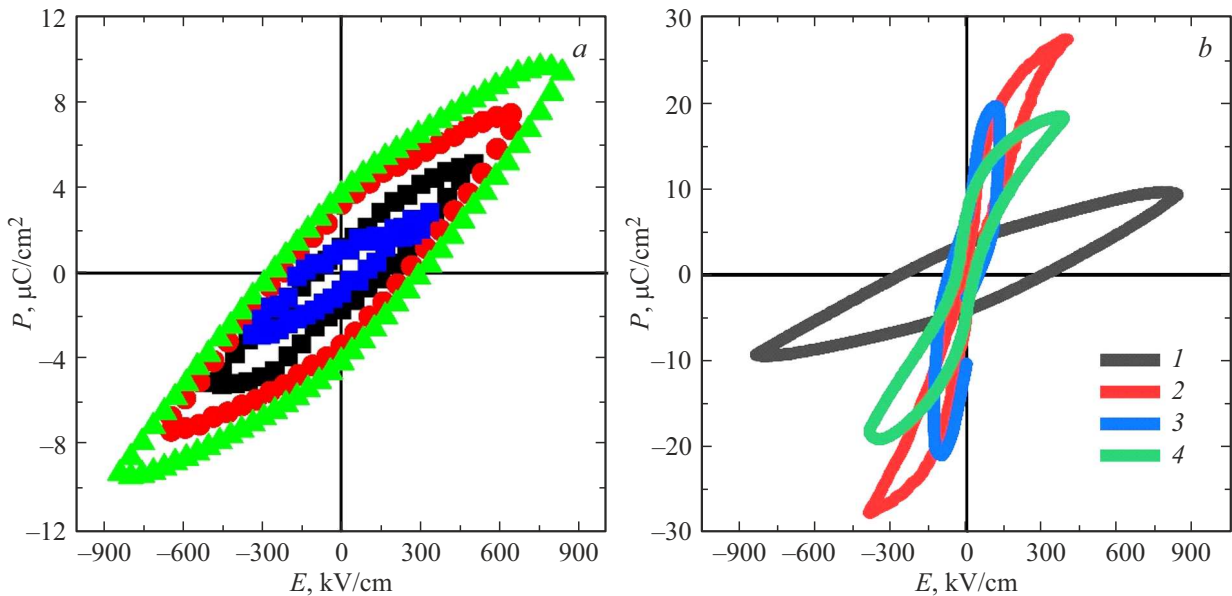


Figure 4. *a* — $P(E)$ dependencies of Ag/Pd/NNSZO/STO heterostructure at temperature of 293 K, frequency of 1 kHz; *b* — $P(E)$ dependence of Ag/Pd/NNSZO/STO heterostructure (1), $0.92\text{NaNbO}_3-0.08\text{SrZrO}_3/\text{SrRuO}_3/\text{SrTiO}_3(001)$ (2) from [17], $0.94\text{NaNbO}_3-0.06\text{SrZrO}_3$ ceramics (3) from [9] and NNSZO/SrRuO₃/MgO(001) (4) from [13].

amplitude of cantilever oscillations was 2 V), the surface potential was measured in the KPFM. From Figure 3, *a* it is clear that the polarization of the regions did not lead to a change in the surface relief of NNSZO film. However, from Figure 3, *b* one can see that on the NNSZO film surface formed polarized regions of different orientations are visualized, i.e. toward the substrate and away from the substrate in [001] direction. The regions were relatively stable — within 60 min they were visualized quite well (the surface potential for both regions decreased in value, while for negative regions faster), after 90 min there were practically no traces of polarized areas on the surface potential scans. Based on the surface potential data of unpolarized fragment

of the film, it is assumed that the film itself has spontaneous polarization, with a predominant direction from the substrate to the film surface (similar to paper [16]). Despite the fact that $0.91\text{NaNbO}_3-0.09\text{SrZrO}_3$ thin films on SrRuO₃/MgO(001) at room temperature according to data in [13] are in the AFE phase, the films obtained in this paper exhibit a response that is more specific to ferroelectrics. This was also supported by the results of measuring the dielectric hysteresis loops in the sample (Figure 4, *a*). For convenience of comparison and analysis of data, Figure 4, *b* shows also $P(E)$ dependencies for $0.94\text{NaNbO}_3-0.06\text{SrZrO}_3$ ceramics from [9] (the closest composition given in publications), for $0.92\text{NaNbO}_3-0.08\text{SrZrO}_3$ film

1 μm thick on SrRuO₃/SrTiO₃(001) from [17], for 0.91NaNbO₃–0.09SrZrO₃ film 900 nm thick on SrRuO₃/MgO(001) from [13] and for heterostructure studied in paper.

When carrying out measurements of this type, especially in thin films, leakage currents play a parasitic role [18]. For this, when measuring $P(E)$ dependencies we try to use the highest possible frequencies (in this case, the leakage current may not have time to develop), and also use special measurement modes with compensation for leakage currents, which complicates the interpretation of the results obtained. This was observed in our case — we did not obtain „classical“ dielectric hysteresis loops for NNSZO 30 nm thick — at values $E > 833$ kV/cm leakage currents began to play significant role, which in some cases resulted in breakdown of the sample. However, in the fields $E > 833$ kV/cm for NNSZO film the $P(E)$ loops turned out to be stable and coincided with each other when measured both in the mode with and without leakage current compensation. This indicates that we are detecting a response associated with the switching of FE polarization in NNSZO film, but not with the effects noted in [19]. For this reason in this paper we used dependencies in the fields $E \leq 833$ kV/cm only. As the electric field strength increases, the P_{\max} values increase monotonically, while P_r and E_c tend to saturate. At $E = 833$ kV/cm typical electrodes have $P_{\max} = 10\text{--}11 \mu\text{C}/\text{cm}^2$, $P_r = 4\text{--}4.5 \mu\text{C}/\text{cm}^2$ and $E_c = 270\text{--}290$ kV/cm).

As Figure 4, b shows that the determined by us type of $P(E)$ dependence significantly differs from both ceramic sample with close composition, and from films 900–1000 nm thick. Paper [9] shows that in $(1-x)\text{NaNbO}_3\text{--}x\text{SrZrO}_3$ SS system with increase in strontium zirconate concentration from 0 to 0.06 value P_{\max} decreases by two times (from 38 to $19 \mu\text{C}/\text{cm}^2$) at background of increase by 3 times of critical field (E_F), inducing the AFE-FE phase transition (from 42 to 116 kV/cm). It is reasonable to assume that in NNSZO ceramics the expected P_{\max} values will be less than $19 \mu\text{C}/\text{cm}^2$, and the E_F values are over 116 kV/cm. The recorded significant increase in E values, necessary for switching polarization during the transition from ceramics to nanoscale films, also occurred, for example, as in the case of the classical ferroelectric BaTiO₃ (from ~ 2.2 to ~ 150 kV/cm [20]) and multiferroic BiFeO₃ (from ~ 40 kV/cm [21] to ~ 250 kV/cm [22]). This, as it is apparent in our case, is associated mainly with the manifestation of strain effects in these materials. Perhaps this also relates to the decrease in P_{\max} in the film we studied in comparison with 0.92NaNbO₃–0.08SrZrO₃ and NNSZO films with thicknesses of 900–1000 nm, however, it was comparable to that in Hf_{0.5}Zr_{0.5}O₂ films with thickness ~ 11 nm at $E \sim 3$ MV/cm (depending on the film annealing temperature P_{\max} varied from 5 to $18 \mu\text{C}/\text{cm}^2$) [23].

The relative permittivity dispersion of the NNSZO film in the frequency range of the measuring electric field $f = 10^3\text{--}10^5$ Hz was insignificant, the values ϵ were ~ 100 . Note that both the $\epsilon(E)$ and $P(E)$ dependencies show a

slight asymmetry. This indicates the presence of internal bias field in NNSZO, which often occurs in heteroepitaxial thin films with large unit cell strain.

4. Conclusion

Using RF cathode deposition 0.91NaNbO₃–0.09SrZrO₃ films 30 nm thick were deposited on SrTiO₃ substrate, the growth of them occurred according to the layer mechanism. This is supported by both the smooth surface relief and the extremely low value of root-mean-square roughness (~ 0.3 nm). Using AFM stable polarized regions were formed on the film surface, which is specific to the ferroelectric phase. According to X-ray diffraction data, the unit cell of the film is significantly stretched in the out-of-plane, which most likely is the reason for the stabilization of the ferroelectric properties in the resulting heterostructure. Further, from our point of view, it is advisable to study in more detail the strain effect on phase transformations in 0.91NaNbO₃–0.09SrZrO₃ thin films.

Funding

The work has been performed under the state assignment of the Southern Scientific Center of Russian Academy of Science, project No. 122020100294-9.

Conflict of interest

The authors have no conflict of interest.

References

- [1] Z. Liu, T. Lu, J. Ye, G. Wang, X. Dong, R. Withers, Y. Liu. *Adv. Mater. Technol.* **3**, 9, 1800111 (2018).
- [2] X. Tan, Ch. Ma, J. Frederick, S. Beckman, K.G. Webber. *J. Am. Ceram. Soc.* **94**, 12, 4091 (2011).
- [3] N. Izyumskaya, Y.-I. Alivov, S.-J. Cho, H. Morkoç, H. Lee, Y.-S. Kang. *Crit. Rev. Solid State Mater. Sci.* **32**, 3–4, 111 (2007).
- [4] European Commission. Directive 2011/65/EU of the European Parliament and of the Council of 8 June 2011 on the restriction of the use of certain hazardous substances in electrical and electronic equipment (recast). *Off. J. Eur. Union* **1**, 88 (2011).
- [5] H.D. Megaw. *Ferroelectrics* **7**, 1, 87 (1974).
- [6] L.E. Cross, B.J. Nicholson. *The London, Edinburgh, and Dublin Phil. Mag. J. Sci.* **46**, 376, 453 (1955).
- [7] A.M. Glazer, H.D. Megaw. *Acta Cryst.* **29**, 5, 489 (1973).
- [8] E.A. Wood, R.C. Miller, J.I. Remeika. *Acta Cryst.* **15**, 1273 (1962).
- [9] H. Guo, H. Shimizu, Y. Mizuno, C.A. Randall. *J. Appl. Phys.* **117**, 21, 214103 (2015).
- [10] H. Shimizu, H. Guo, S.E. Reyes-Lillo, Y. Mizuno, K.M. Rabe, C.A. Randall. *Dalton Trans.* **44**, 23, 10763 (2015).
- [11] I. Fujii, T. Shimasaki, T. Nobe, H. Adachi, T. Wada. *Jpn. J. Appl. Phys.* **57**, 11S, 11UF13 (2018).

- [12] A.V. Pavlenko, S.P. Zinchenko, D.V. Stryukov, A.P. Kovtun, Nanorazmernye plenki niobata bariya-strontsiya: osobennosti polucheniya v plazme vysokochasotnogo razryada, struktura i fizicheskie svoystva. Izdatelstvo YuNTs RAN, Rostov-na-Donu (2022). 244 s. (in Russian)
- [13] A.V. Pavlenko, D.V. Stryukov, V.G. Smotrakov, E.V. Glazunova, Yu.A. Kuprina, N.V. Ter-Oganessian. *Ferroelectrics* **590**, 1, 227 (2022).
- [14] A.R. Shugurov, A.V. Panin. *ZhTF* **90**, 12, 1971, (2020). (in Russian).
- [15] P.E. Janolin. *J. Mater. Sci.* **44**, 5025 (2009).
- [16] A.V. Pavlenko, D.A. Kiselev, Ya.Yu. Matyash, *FTT* **63**, 6, 776 (2021). (in Russian).
- [17] K. Beppu, T. Shimasaki, I. Fujii, T. Imai, H. Adachi, T. Wada. *Phys. Lett. A* **384**, 27, 126690 (2020).
- [18] R. Meyer, R. Waser, K. Prume, T. Schmitz, S. Tiedke. *Appl. Phys. Lett.* **86**, 14, 142907 (2005).
- [19] J.F. Scott. *J. Phys.: Condens. Matter* **20**, 2, 021001 (2007).
- [20] K.J. Choi, M. Biegalski, Y.L. Li, A. Sharan, J. Schubert, R. Uecker, P. Reiche, Y.B. Chen, X.Q. Pan, V. Gopalan, L.-Q. Chen, D.G. Schlom, C.B. Eom. *Science* **306**, 5698, 1005 (2004).
- [21] D. Lebeugle, D. Colson, A. Forget, M. Viret. *Appl. Phys. Lett.* **91**, 2, 022907 (2007).
- [22] J. Li, J. Wang, M. Wuttig, R. Ramesh, N. Wang, B. Ruetter, A.P. Pyatakov, A.K. Zvezdin, D. Viehland. *Appl. Phys. Lett.* **84**, 25, 5261 (2004).
- [23] Y.H. Lee, H.J. Kim, T. Moon, K.D. Kim, S.D. Hyun, H.W. Park, Y.B. Lee, M.H. Park C.S. Hwang. *Nanotechnology* **28**, 30, 305703 (2017).

Translated by I.Mazurov